energies

MDPI

Article

Stability and Thermal Properties Study of Metal Chalcogenide-Based Nanofluids for Concentrating Solar Power †

Paloma Martínez-Merino, Rodrigo Alcántara, Teresa Aguilar, Juan Jesús Gallardo, Iván Carrillo-Berdugo, Roberto Gómez-Villarejo, Mabel Rodríguez-Fernández and Javier Navas *

Departamento de Química Física, Facultad de Ciencias, Universidad de Cádiz, E-11510 Cádiz, Spain; paloma.martinez@uca.es (P.M.-M.); rodrigo.alcantara@uca.es (R.A.); mariateresa.aguilar@uca.es (T.A.); jj.gallardo@uca.es (J.J.G.); ivan.carrillo@uca.es (I.C.-B.); roberto.gomezvi@uca.es (R.G.-V.); mariaisabel.rodriferna@alum.uca.es (M.R.-F.)

* Correspondence: javier.navas@uca.es

† This paper is an extended version of our paper entitled "Stability and thermal properties study of 2D-metal chalcogenides-based nanofluids for concentrating solar power" published in 1st International Conference on Nanofluids (ICNf2019) and 2nd European Symposium on Nanofluids (ESNf2019), Castelló, Spain, 26–28 June 2019; pp. 182–185.

Received: 30 October 2019; Accepted: 2 December 2019; Published: 6 December 2019

Abstract: Nanofluids are colloidal suspensions of nanomaterials in a fluid which exhibit enhanced thermophysical properties compared to conventional fluids. The addition of nanomaterials to a fluid can increase the thermal conductivity, isobaric-specific heat, diffusivity, and the convective heat transfer coefficient of the original fluid. For this reason, nanofluids have been studied over the last decades in many fields such as biomedicine, industrial cooling, nuclear reactors, and also in solar thermal applications. In this paper, we report the preparation and characterization of nanofluids based on one-dimensional MoS_2 and WS_2 nanosheets to improve the thermal properties of the heat transfer fluid currently used in concentrating solar plants (CSP). A comparative study of both types of nanofluids was performed for explaining the influence of nanostructure morphologies on nanofluid stability and thermal properties. The nanofluids prepared in this work present a high stability over time and thermal conductivity enhancements of up to 46% for MoS_2-based nanofluid and up to 35% for WS_2-based nanofluid. These results led to an increase in the efficiency of the solar collectors of 21.3% and 16.8% when the nanofluids based on MoS_2 nanowires or WS_2 nanosheets were used instead of the typical thermal oil.

Keywords: nanofluids; heat transfer fluid (HTF); concentrating solar power (CSP); parabolic trough collector (PTC); nanowires; nanosheets; stability; thermophysical properties

1. Introduction

Over the last decades, the interest around renewable energies has increased due to the increasing energy demand and the environmental problems derived from fossil fuels combustion. In this scenario, solar energy presents a high potential to supply the primary energy demand, although the technology to harvest and store solar radiation needs to advance to make it affordable in comparison with fossil-based electricity. Currently, there are two technologies for power generation based on solar energy: concentrating solar power (CSP) and photovoltaics (PVs). The CSP systems present a higher potential to store energy in comparison with PV systems [1]. As a result, CSP with a thermal energy storage (TES) system is considered the first choice to provide electricity on a large scale, even at nighttime or on cloudy days [2,3]. The principle behind CSP consists of the reflection of solar

irradiation in a small area where heat is collected by a fluid and, subsequently, used in a Rankine cycle to generate steam. Finally, the steam drives a turbine which powers a generator to produce electricity [4–6]. Among the different solar collectors, parabolic trough collectors (PTCs) are the most installed technology worldwide [7]. In PTC technology, a group of curved reflectors focus sunrays onto an absorber tube which is located in the focal line of collectors. This tube contains the heat transfer fluid (HTF) which collects and transports the thermal energy to electricity generation systems or to storage facilities [8–10].

One of the research lines to increase the efficiency in CSP plants based on PTCs is replacing the HTF (water or oil) with nanofluids. Typically, nanofluids, which are nanocolloidal suspensions of particles in a fluid, present improved thermophysical properties compared to conventional fluids. Tyagi et al. [11] predicted a 10% increment in the efficiency of solar collectors when nanofluids of aluminum are used as the working fluid. Also, an analysis of the applicability of nanofluids of graphite, aluminum, copper, and silver at tower solar power collectors has been reported with interesting results. Nanofluids based on these nanoparticles were analyzed for use in direct absorption solar collectors, and an efficiency improvement of up to 10% was found [12]. As regards PTCs, Mwesigye et al. [13] discovered an improvement in thermal efficiency of 7% with the use of a nanofluid based on Al_2O_3 nanoparticles. Nevertheless, the number of works on nanofluids prepared with the eutectic mixture of biphenyl and diphenyl oxide, which is the typical organic oil used in CSP plants, is very small. Furthermore, there are few works on nanofluids based on one-dimensional and two-dimensional nanomaterials such as those offered in this study.

In this paper, we used the eutectic mixture of biphenyl and diphenyl oxide as a base fluid to prepare nanofluids based on metal chalcogenides. Because an important challenge is to obtain stable nanofluids over time, the initial aim was to prepare bidimensional nanostructures of metal chalcogenides suspended in HTF. The highest aspect ratio of nanosheets avoids the common sedimentation observed in spherical nanoparticles. Both MoS_2 and WS_2 materials present high thermal conductivities (34.5 $Wm^{-1}K^{-1}$ and 32 $Wm^{-1}K^{-1}$) and a hexagonal structure which facilitates its exfoliation in nanosheets [14–16]. Moreover, polyethylene glycol (PEG) was used as surfactant since its efficiency in HTF systems was proven in a previous work [17]. However, unexpectedly, in the case of MoS_2 instead of nanosheets, the resulting nanomaterial obtained after liquid phase exfoliation (LPE) were nanowires. Therefore, during the present work, a comprehensive study was performed on the influence of the morphology of metal chalcogenide nanostructures in the stability and thermal improvements of nanofluids.

2. Materials and Methods

2.1. Reagents

WS_2 (nanopowder, 90 nm), MoS_2 (powder, <2 μm), and polyethylene glycol-200 (PEG) were purchased from Sigma–Aldrich. The HTF employed to prepare the nanofluids was the eutectic mixture of biphenyl (26.5%) and diphenyl oxide (73.5%) typically used in PTC plants. The commercial brand name of this eutectic mixture is Dowtherm A, and it was supplied by Dow Chemical Company©. All chemicals were used without further purification.

2.2. Preparation of MoS_2- and WS_2-Based Nanofluids

Liquid phase exfoliation was used to prepare the metal chalcogenide-based nanofluids. In this process, 15 mg of metal chalcogenide (MoS_2 or WS_2) were weighed and add to four vials. Then, 5 mL of a solution with a mass concentration of 0.20 wt.% PEG in HTF was added to each vial. The vials were introduced to an Elmasonic-P ultrasonic bath, and 80 kHz of frequency was applied for 4 h. After that, black-colored solutions were centrifuged at 1000 rpm for 10 min. The precipitates were discarded, and the supernatants were subjected to another centrifugation at 400 rpm for 10 min to remove non-exfoliated nanomaterial. The supernatant liquid obtained in the second centrifugation was the final nanofluid.

2.3. Characterization of Nanofluids

The nanofluids prepared were characterized to study their stability and thermal properties. Both types of characterization are essential to elucidate their application in CSP plants. Also, transmission electron microscopy was used to study the size and morphology of the nanostructures present in both nanofluids using a JEM-2100F microscope supplied by Jeol®. The stability of nanofluids was studied over a week by means of UV-Vis spectroscopy and dynamic light scattering (DLS). The UV-Vis spectra were registered between 400 and 850 nm using a USB2000+ spectrometer and an Ocean Optics® DH-2000-BAL halogen lamp. The evolution of the extinction coefficient was performed at 678 nm for MoS_2 and 629 nm for WS_2 where there are characteristics bands for these metal chalcogenides [18,19]. Dynamic light scattering was performed to determine the hydrodynamic particle size evolution over time. The equipment used to perform the DLS measurements was a Zetasizer Nano ZS system supplied by Malvern Instruments Ltd®.

Thermal conductivity (k) was determined using the equation $k(T) = D(T)\cdot C_P(T)\cdot\rho(T)$, where D is the thermal diffusivity, C_P is the isobaric specific heat, and ρ is the density which was defined in ASTM E 1461-01. Thermal diffusivity measurements were performed using LFA 467 equipment, supplied by NETZSCH, and conducted using the light flash technique. Temperature-modulated differential scanning calorimeter (TMDSC) technique was performed in a DSC 214 Polyma, supplied by NETZSCH, to determine the isobaric specific heat. The program established to perform isobaric specific heat measurements has been described previously [17]. Density values were determined by pycnometry. In addition, dynamic viscosity was studied due to the fact of its influence in the heat transfer process [20–22]. Dynamic viscosity measurements were obtained using a vibrational viscometer, model SV-10, supplied by A&D Company Ltd. The aforementioned thermal and rheological properties of nanofluids and HTF were analyzed in a temperature range from 290 K to 370 K.

3. Results

3.1. Morphological and Size Characterization of WS_2 and MoS_2 Nanostructures

Although MoS_2 and WS_2 are metal sulfides with similar properties, and the nanofluids were prepared with the same methodology, the TEM images revealed unexpected morphological results. Figure 1a shows the nanostructures found in the WS_2 nanofluid after LPE. We can observe nanosheets with lateral dimensions between 45 and 70 nm. However, in the MoS_2 nanofluid, the nanostructures obtained were nanowires as observed in Figure 1b. This is a surprising result, since the LPE process is typically used to obtain nanosheets from bulk material [23–26]. The nanowires obtained presented a diameter of approximately 27 nm and a 700 nm length (see Figure 1b). Inevitably, this morphological difference influenced the rest of the studied properties of nanofluids. On the other hand, the XRD patterns were registered for the MoS_2 and WS_2 solids extracted from the nanofluid after the LPE process. Figure 2 shows the patterns obtained. In both cases, we can observe that the pattern was typical for the hexagonal space group P63/mmc. The assignation of the planes according to the references (JCPDS cards No. 37-1492 and No. 08-0237 for MoS_2 and WS_2, respectively) is observed in the patterns shown in Figure 2.

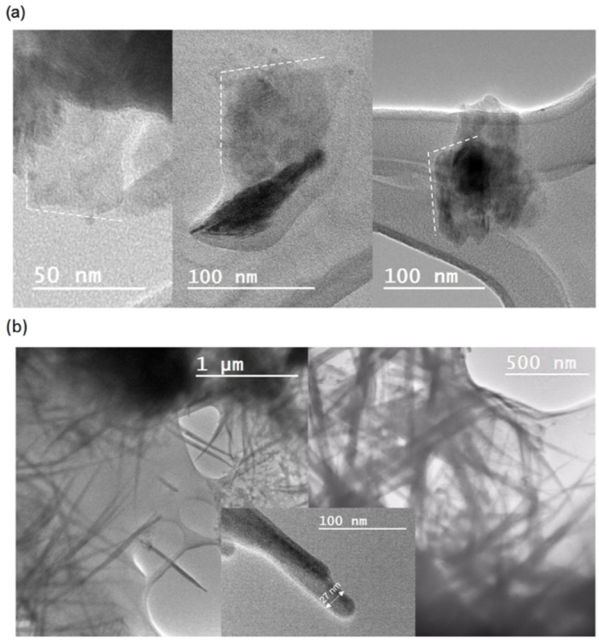

Figure 1. TEM images of WS_2 nanosheets (**a**) and MoS_2 nanowires (**b**) obtained after the liquid phase exfoliation (LPE) process.

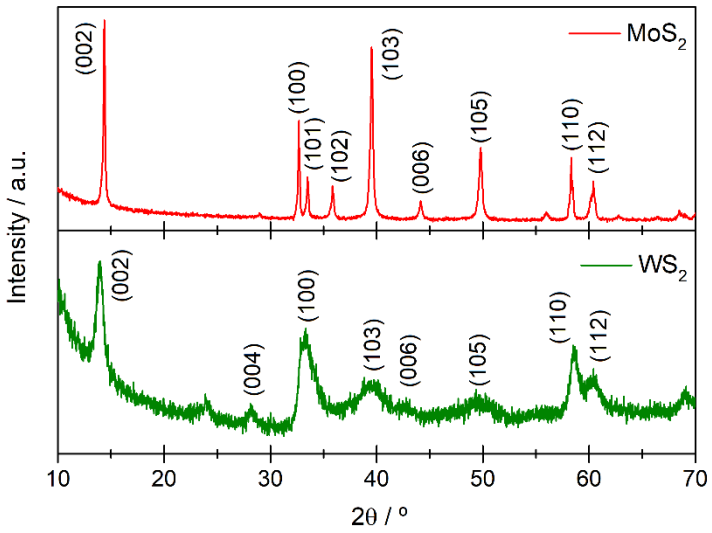

Figure 2. XRD patterns of MoS_2 nanowires and WS_2 nanosheets obtained after the LPE process.

3.2. Stability of Nanofluids

The stability study showed low levels of sedimentation over time for both nanofluids according to DLS and UV-Vis measurements. Figure 3a shows that, after three days of nanofluids preparation, the extinction coefficient was constant and, therefore, nanofluids began to stabilize. At the end of the characterization, the extinction coefficient at 678 nm in MoS_2 nanofluid decreased by 13%. For the WS_2 nanofluid, the decrease in extinction coefficient at 629 nm was 22%. As can be seen, the WS_2 nanofluid exhibited a higher extinction coefficient which suggests that a higher amount of nanomaterial was exfoliated during the LPE process. These results are concordant with those obtained by DLS technique (Figure 3b). The average hydrodynamic particle size found in WS_2 nanofluids was 200 nm, and it remained stable over the characterization time. Otherwise, in MoS_2 nanofluid, the average hydrodynamic particle size increased from 350 nm to 530 nm. Thus, in WS_2 nanofluid, the smaller particle size over time revealed that the agglomeration phenomenon and sedimentation process were not as prominent as in the MoS_2 nanofluid which led to a greater concentration of WS_2 nanostructures

dispersed in HTF. In the case of MoS_2 nanofluids, the larger particle size would explain the lower extinction coefficient values of nanostructures present in the nanofluid compared to the WS_2 nanofluid, notwithstanding that at the end of the characterization, the agglomerates were not large enough for sedimentation to occur, since the extinction coefficient remained constant. Also, Figure 4 shows the UV-Vis spectra registered for both nanofluids right after preparation and seven days later in order to analyze shifts in the typical peaks observed for MoS_2 and WS_2. We can observe a decrease in the intensity of the spectra, but no significant shift of the absorption bands can be observed.

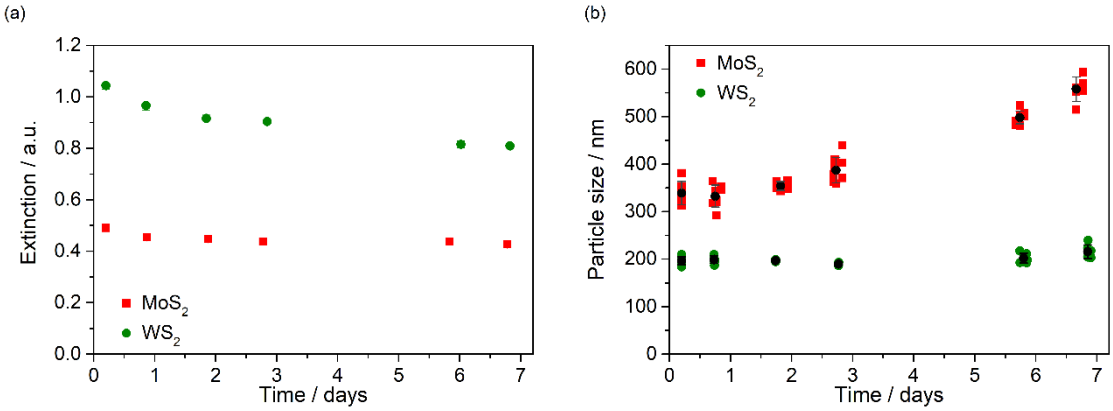

Figure 3. Extinction coefficient evolution obtained from UV-Vis spectra (**a**) and particle size results obtained from the DLS technique (**b**) for seven days.

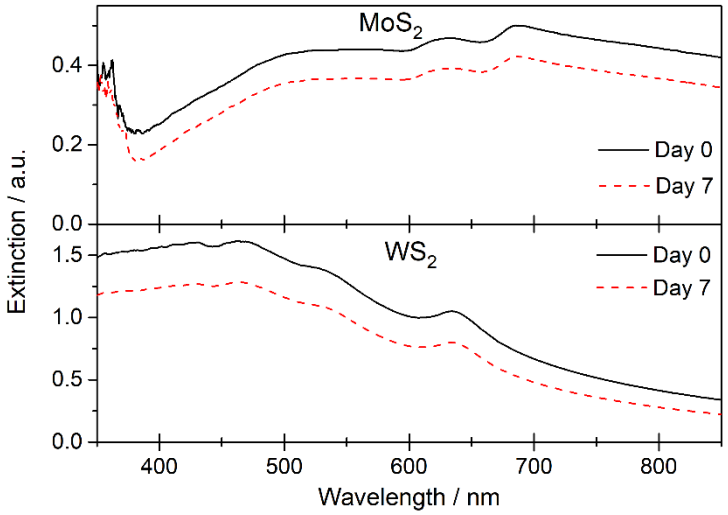

Figure 4. UV-Vis spectra for MoS_2- and WS_2-based nanofluids right after preparation and seven days later.

3.3. Nanofluid Performance

Some properties of nanofluids show a clear influence on heat transfer processes such as density, viscosity, isobaric specific heat, and thermal conductivity. In the case of density, an increase in density led to an enhancement in the heat transfer process. Also, it was expected that the nanofluid density was higher than the density of the base fluid, because density of liquids is lower than that of solids. As is observed in Table 1, WS_2 and MoS_2 nanofluids exhibited a slight increment in density values with respect to the pure HTF. This is a positive feature due to the high density values improving thermal conductivity [27–29]. In addition, the higher increase of density in WS_2 nanofluid was related to the higher nanostructure concentration. According to dynamic viscosity measurements, the values were close to that of HTF. The maximum increase in viscosity was 3.2% for MoS_2 nanofluid. However,

these slight increases in viscosity were not significant enough to cause changes in pumping power or heat transfer.

Table 1. Density and dynamic viscosity results obtained for the base fluid and for the metal sulphide-based nanofluids at 298 K.

Sample	Density/kg m^{-3}	Dynamic viscosity /mPa s
HTF	1056.6 ± 0.5	3.70 ± 0.02
Nanofluid of MoS_2	1061.6 ± 0.2	3.82 ± 0.02
Nanofluid of WS_2	1069.3 ± 0.7	3.77 ± 0.01

Figure 5 shows the isobaric specific heat values obtained for nanofluids and base fluid. The highest increase of isobaric specific heat was up to 4.7% for MoS_2 nanofluid and up to 1.2% for WS_2 nanofluid with respect to HTF at 363 K. These results suggest that there was not a noticeable increase of this property which is understandable taking into account that isobaric specific heat of solids is lower than that of liquids. Furthermore, classic models based on mixture theory predict a decrease of isobaric-specific heat in respect to base fluid [30–32]. Notwithstanding, some recent theories do not consider nanofluids as a mixture of solid and liquid to determine the isobaric specific heat of nanofluids. These theories also include the study of the interaction between the molecules of nanostructure, surfactant, and liquid as a key factor in the enhancement of thermal resistance in the nanostructure/liquid interface [33–36]. Thus, these recent studies would explain the increase of isobaric-specific heat of nanofluids in respect to base fluid as it is reported in this paper and in previous works [37,38].

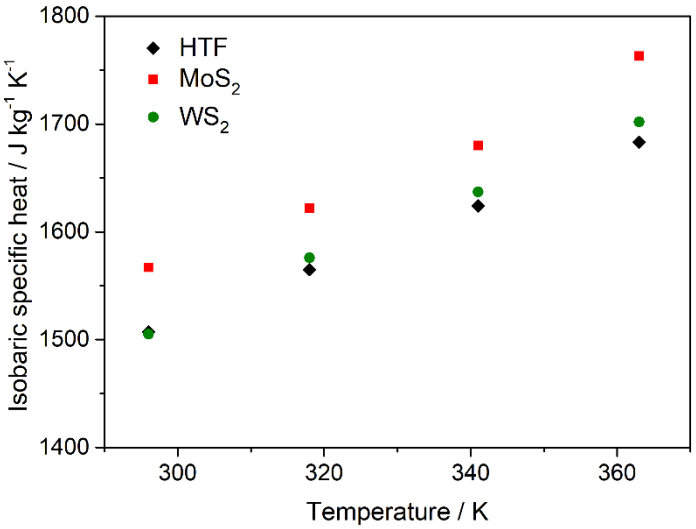

Figure 5. Isobaric-specific heat values of nanofluids and HTF.

Finally, the thermal conductivity of nanofluids and HTF was determined indirectly from the formula $k(T) = D(T)\cdot C_P(T)\cdot\rho(T)$ which considers thermal diffusivity (D), isobaric specific heat (C_P), and density (ρ). Figure 6a shows the thermal conductivity values of the nanofluids and the pure HTF for comparison. We can observe a different trend with temperature for nanofluids; that is, the thermal conductivity increases with temperature for nanofluids, while it decreases for the pure HTF. This opposite trend is favorable for the use of nanofluids in CSP plants, where high temperatures are used in operating conditions. This can be explained because, at high temperature, the collisions among nanostructures and between nanostructures and HTF molecules are intensified which leads to an increase in the Brownian motion and contributes to thermal conductivity enhancement. Figure 6b shows the thermal conductivity enhancement (TCE) calculated according to $TCE(\%) = \left(\frac{(k_{nf}-k_{bf})}{k_{bf}}\right)\times 100$.

A maximum increase of 45.6% for the nanofluid based on MoS_2 nanowires and 34.5% for the nanofluid based on WS_2 at 363 K were observed. Here, although bulk solids present similar thermal conductivities, as are shown above, the increase in the thermal conductivity values for nanofluids were different. Particularly interesting is that nanofluids based on MoS_2 with less concentration of nanostructure dispersed on HTF presented the largest thermal conductivity enhancement. A plausible reason for this phenomenon lies in the size and morphology of the nanostructures present in nanofluids. As observed during the DLS study, the stable agglomerates of MoS_2 nanowires were larger than the WS_2 nanosheet agglomerates. This greater agglomeration of nanowires in MoS_2 nanofluid can lead to percolation pathways that improve thermal conductivity more significantly than the well-distributed WS_2 nanosheets.

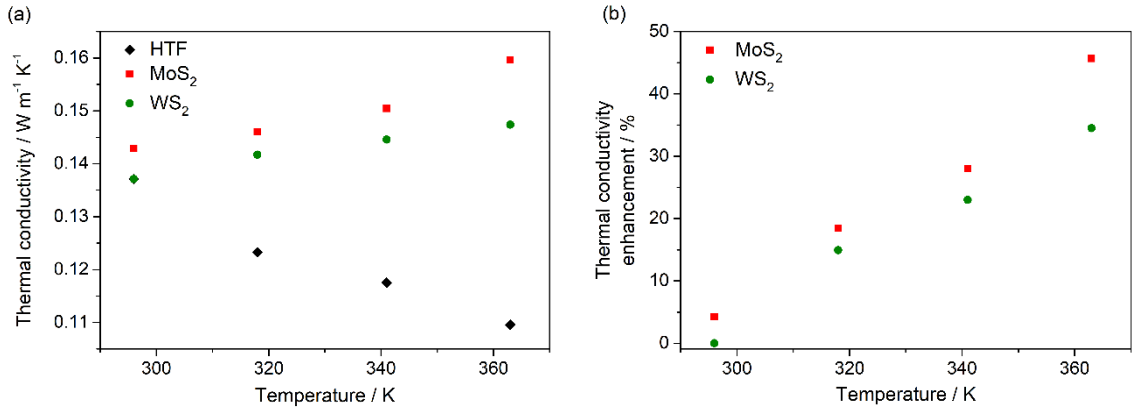

Figure 6. Thermal conductivity of base fluid and nanofluids (**a**) and the enhancement of the thermal conductivity for nanofluids (**b**).

In order to assess the efficiency of nanofluids in a CSP plant, the temperature of nanofluids and HTF at the heat pipe outlet was estimated. This temperature should be higher in nanofluids than in HTF if the heat transfer is improved. Mathematically, the heat flux between the surface of the pipe and the fluid, q_s'', is expressed as $q_s'' = h\Delta T = h(T_s - T_{m,0})$, where h is the heat transfer coefficient, T_s is the pipe surface temperature, and $T_{m,0}$ is the temperature of the fluid at the pipe outlet [39]. In this equation, for a constant solar irradiance of 1000 W m^{-2}, q_s'' and T_s are considered, and the ΔT for both the base fluid and for the nanofluids can be compared ($\Delta T_{nf}/\Delta T_{bf} = h_{bf}/h_{nf}$). In addition, the heat transfer coefficient can be estimated following the Mouromtseff number: $Mo = h = \left(\rho^{0.8} k^{0.67} C_P^{0.33}\right)/\mu^{0.47}$. Thus, Figure 7 shows the ratio of the Mouromtseff numbers of the nanofluids and the base fluid, which gives an idea of the enhancement of the heat transfer coefficient of the nanofluids analyzed. An increase up to 29% was observed. Finally, if $\Delta T_{nf}/\Delta T_{bf}1$, the outlet temperature $T_{m,0}$ was higher when a nanofluid was used with respect to HTF, and the efficiency of the collectors was improved. Figure 8 shows that MoS_2 and WS_2 nanofluids present higher outlet temperatures than HTF, since $\Delta T_{nf}/\Delta T_{bf}$ was lower than 1 in both cases. By increasing the temperature in the pipe, the difference in the outlet temperature of the nanofluid was accentuated with respect to HTF, improving the efficiency of the collector up to 21.3% at 363 K. The greater thermal conductivity and isobaric-specific heat of the nanofluid based on MoS_2 nanowires contributed to the outlet temperature rising up to 5% more than in the nanofluid based on WS_2 nanosheets.

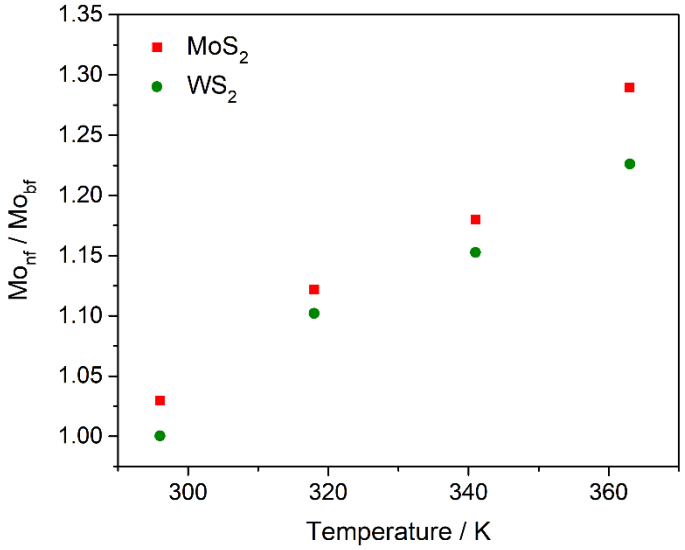

Figure 7. Ratio of the Mouromtseff numbers of the nanofluids prepared and the base fluid.

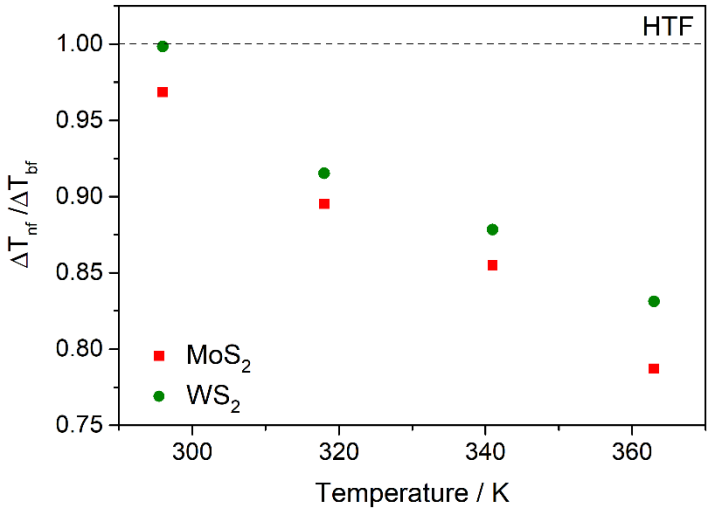

Figure 8. Comparison of the outlet temperature in solar collectors when metal sulfide nanofluids are used.

4. Conclusions

The LPE process was used in this work to prepare nanofluids based on WS_2 and MoS_2 nanostructures for their application as heat transfer fluids in CSP plants based on parabolic trough collectors. Thus, the base fluid used for nanofluids preparation was the eutectic mixture of diphenyl oxide and biphenyl commonly found in CSP plants.

The most striking result was that WS_2 and MoS_2 exhibited different behaviors during the same exfoliation process, and two different types of nanostructures were obtained: MoS_2 nanowires and WS_2 nanosheets. According to DLS and UV-Vis spectroscopy, nanofluids based on MoS_2 nanowires and WS_2 nanosheets presented a high stability over time which suggests that this kind of advanced nanomaterials can be an alternative to nanofluids based on spherical nanoparticles. In the nanofluid based on WS_2 nanosheets, the concentration of nanomaterial was higher, and agglomerates were smaller than in the nanofluid based on MoS_2 nanowires. Nevertheless, nanofluid based on MoS_2 nanowires exhibited a greater improvement of thermal properties despite the lower concentration of nanostructures dispersed in HTF compared to the WS_2 nanofluid and the similar thermal conductivity of the metal chalcogenides. The larger agglomerates of MoS_2 nanowires led to percolation paths

through which heat was transferred faster and more efficiently than through the well-distributed WS_2 nanosheets.

Notwithstanding, both nanofluids presented significant improvements in the heat transfer process with respect to HTF. Thus, the thermal conductivity increased up to 45.6% in the nanofluid based on MoS_2 nanowires and 34.5% in the nanofluid based on WS_2. In addition, isobaric-specific heat was measured and a slight increase of up to 4.7% for MoS_2 nanofluid and 1.2% for WS_2 nanofluid were obtained which is consistent with the current isobaric-specific models. Finally, the nanofluid temperatures at the outlet of the absorber tube used in CSP plants were estimated and compared with that obtained for the pure HTF. The results revealed that the efficiency of the collector was increased up to 21.3% and 16.8% when the MoS_2 or WS_2 nanofluids were used, respectively. Therefore, nanofluids based on metal chalcogenides show properties of great interest to be used in CSP plants based on parabolic trough collectors, such as their high stability and their thermophysical properties improvements, compared to those of the heat transfer fluid currently used.

Author Contributions: Methodology, P.M.-M., T.A., J.J.G., I.C.-B., R.G.-V.; investigation, P.M.-M., R.A., M.R.-F.; writing—original draft preparation, P.M.-M.; writing—review and editing, J.N.; supervision, J.N.; project administration, J.N.; funding acquisition, J.N.

Funding: This research was funded by Ministerio de Ciencias, Innovación y Universidades (Spanish Government), grant numbers RTI2018-096393-B-I00 and UNCA15-CE-2945. The APC was funded by Nanouptake COST Action CA15119.

Acknowledgments: This investigation was a contribution to the COST (European Cooperation in Science and Technology) Action CA15119: Overcoming Barriers to Nanofluids Market Uptake (NanoUptake). P.M.-M. acknowledges the EU COST Action CA15119: Overcoming Barriers to Nanofluids Market Uptake for financial support in the participation of the 1st International Conference on Nanofluids (ICNf) and the 2nd European Symposium on Nanofluids (ESNf) participation.

Conflicts of Interest: The authors declare no conflict of interest.

References

1. Desideri, U.; Campana, P.E. Analysis and comparison between a concentrating solar and a photovoltaic power plant. *Appl. Energy* **2014**, *113*, 422–433. [CrossRef]
2. Xu, B.; Li, P.W.; Chan, C. Application of phase change materials for thermal Energyy storage in concentrated solar thermal power plants: A review to recent developments. *Appl. Energy* **2015**, *160*, 286–307. [CrossRef]
3. Rovense, F.; Reyes-Belmonte, M.A.; Gonzalez-Aguilar, J.; Amelio, M.; Bova, S.; Romero, M. Flexible electricity dispatch for CSP plant using un-fired closed air Brayton cycle with particles based thermal Energyy storage system. *Energy* **2019**, *173*, 971–984. [CrossRef]
4. Zhang, H.L.; Baeyens, J.; Degreve, J.; Caceres, G. Concentrated solar power plants: Review and design methodology. *Renew. Sust. Energy Rev.* **2013**, *22*, 466–481. [CrossRef]
5. Islam, M.T.; Huda, N.; Abdullah, A.B.; Saidur, R. A comprehensive review of state-of-the-art concentrating solar power (CSP) technologies: Current status and research trends. *Renew. Sust. Energy Rev.* **2018**, *91*, 987–1018. [CrossRef]
6. Liu, M.; Tay, N.H.S.; Bell, S.; Belusko, M.; Jacob, R.; Will, G.; Saman, W.; Bruno, F. Review on concentrating solar power plants and new developments in high temperature thermal Energyy storage technologies. *Renew. Sust. Energy Rev.* **2016**, *53*, 1411–1432. [CrossRef]
7. Wang, F.Q.; Cheng, Z.M.; Tan, J.Y.; Yuan, Y.; Shuai, Y.; Liu, L.H. Progress in concentrated solar power technology with parabolic trough collector system: A comprehensive review. *Renew. Sust. Energy Rev.* **2017**, *79*, 1314–1328.
8. Fernandez-Garcia, A.; Zarza, E.; Valenzuela, L.; Perez, M. Parabolic-trough solar collectors and their applications. *Renew. Sust. Energy Rev.* **2010**, *14*, 1695–1721. [CrossRef]
9. Price, H.; Lupfert, E.; Kearney, D.; Zarza, E.; Cohen, G.; Gee, R.; Mahoney, R. Advances in parabolic trough solar power technology. *J. Sol. Energy T Asme* **2002**, *124*, 109–125. [CrossRef]
10. Morin, G.; Dersch, J.; Platzer, W.; Eck, M.; Haberle, A. Comparison of Linear Fresnel and Parabolic Trough Collector power plants. *Sol. Energy* **2012**, *86*, 1–12. [CrossRef]

11. Tyagi, H.; Phelan, P.; Prasher, R. Predicted Efficiency of a Low-Temperature Nanofluid-Based Direct Absorption Solar Collector. *J. Sol. Energy Eng.* **2009**, *131*, 041004. [CrossRef]
12. Taylor, R.A.; Phelan, P.E.; Otanicar, T.P.; Walker, C.A.; Nguyen, M.; Trimble, S.; Prasher, R. Applicability of nanofluids in high flux solar collectors. *J. Renew. Sustain. Energy* **2011**, *3*, 023104. [CrossRef]
13. Mwesigye, A.; Huan, Z.J.; Meyer, J.P. Thermodynamic optimisation of the performance of a parabolic trough receiver using synthetic oil-Al2O3 nanofluid. *Appl. Energy* **2015**, *156*, 398–412. [CrossRef]
14. Peng, B.; Zhang, H.; Shao, H.Z.; Xu, Y.C.; Zhang, X.C.; Zhu, H.Y. Thermal conductivity of monolayer MoS2, MoSe2, and WS2: Interplay of mass effect, interatomic bonding and anharmonicity. *RSC Adv.* **2016**, *6*, 5767–5773. [CrossRef]
15. Peimyoo, N.; Shang, J.Z.; Yang, W.H.; Wang, Y.L.; Cong, C.X.; Yu, T. Thermal conductivity determination of suspended mono- and bilayer WS2 by Raman spectroscopy. *Nano Res.* **2015**, *8*, 1210–1221. [CrossRef]
16. Yan, R.S.; Simpson, J.R.; Bertolazzi, S.; Brivio, J.; Watson, M.; Wu, X.F.; Kis, A.; Luo, T.F.; Walker, A.R.H.; Xing, H.G. Thermal Conductivity of Monolayer Molybdenum Disulfide Obtained from Temperature-Dependent Raman Spectroscopy. *ACS Nano* **2014**, *8*, 986–993. [CrossRef]
17. Navas, J.; Sanchez-Coronilla, A.; Martin, E.I.; Teruel, M.; Gallardo, J.J.; Aguilar, T.; Gomez-Villarejo, R.; Alcantara, R.; Fernandez-Lorenzo, C.; Pinero, J.C.; et al. On the enhancement of heat transfer fluid for concentrating solar power using Cu and Ni nanofluids: An experimental and molecular dynamics study. *Nano Energy* **2016**, *27*, 213–224. [CrossRef]
18. Mishra, A.K.; Lakshmi, K.V.; Huang, L.P. Eco-friendly synthesis of metal dichalcogenides nanosheets and their environmental remediation potential driven by visible light. *Sci. Rep. UK* **2015**, *5*, 15718. [CrossRef]
19. Song, H.L.; Yu, X.F.; Chen, M.; Qiao, M.; Wang, T.J.; Zhang, J.; Liu, Y.; Liu, P.; Wang, X.L. Modification of WS2 nanosheets with controllable layers via oxygen ion irradiation. *Appl. Surf. Sci.* **2018**, *439*, 240–245. [CrossRef]
20. Murshed, S.M.S.; Leong, K.C.; Yang, C. Investigations of thermal conductivity and viscosity of nanofluids. *Int. J. Therm. Sci.* **2008**, *47*, 560–568. [CrossRef]
21. Prasher, R.; Song, D.; Wang, J.L.; Phelan, P. Measurements of nanofluid viscosity and its implications for thermal applications. *Appl. Phys. Lett.* **2006**, *89*, 133108. [CrossRef]
22. Khanafer, K.; Vafai, K. A critical synthesis of thermophysical characteristics of nanofluids. *Int. J. Heat Mass Trans.* **2011**, *54*, 4410–4428. [CrossRef]
23. Shen, J.F.; He, Y.M.; Wu, J.J.; Gao, C.T.; Keyshar, K.; Zhang, X.; Yang, Y.C.; Ye, M.X.; Vajtai, R.; Lou, J.; et al. Liquid Phase Exfoliation of Two-Dimensional Materials by Directly Probing and Matching Surface Tension Components. *Nano Lett.* **2015**, *15*, 5449–5454. [CrossRef] [PubMed]
24. Teruel, M.; Aguilar, T.; Martinez-Merino, P.; Carrillo-Berdugo, I.; Gallardo-Bernal, J.J.; Gomez-Villarejo, R.; Alcantara, R.; Fernandez-Lorenzo, C.; Navas, J. 2D MoSe2-based nanofluids prepared by liquid phase exfoliation for heat transfer applications in concentrating solar power. *Sol. Energy Mat. Sol. Cells* **2019**, *200*, 109972. [CrossRef]
25. Lotya, M.; Hernandez, Y.; King, P.J.; Smith, R.J.; Nicolosi, V.; Karlsson, L.S.; Blighe, F.M.; De, S.; Wang, Z.M.; McGovern, I.T.; et al. Liquid Phase Production of Graphene by Exfoliation of Graphite in Surfactant/Water Solutions. *J. Am. Chem. Soc.* **2009**, *131*, 3611–3620. [CrossRef]
26. Nicolosi, V.; Chhowalla, M.; Kanatzidis, M.G.; Strano, M.S.; Coleman, J.N. Liquid Exfoliation of Layered Materials. *Science* **2013**, *340*, 1226419. [CrossRef]
27. Keblinski, P.; Eastman, J.A.; Cahill, D.G. Nanofluids for thermal transport. *Mater. Today* **2005**, *8*, 36–44. [CrossRef]
28. Timofeeva, E.V.; Yu, W.H.; France, D.M.; Singh, D.; Routbort, J.L. Nanofluids for heat transfer: An engineering approach. *Nanoscale Res. Lett.* **2011**, *6*, 182. [CrossRef]
29. Mohammed, H.A.; Hasan, H.A.; Wahid, M.A. Heat transfer enhancement of nanofluids in a double pipe heat exchanger with louvered strip inserts. *Int. Commun. Heat Mass* **2013**, *40*, 36–46. [CrossRef]
30. Taylor, R.; Coulombe, S.; Otanicar, T.; Phelan, P.; Gunawan, A.; Lv, W.; Rosengarten, G.; Prasher, R.; Tyagi, H. Critical Review of the Novel Applications and Uses of Nanofluids. In Proceedings of the Asme Micro/Nanoscale Heat and Mass Transfer International Conference, Atlanta, GA, USA, 3–6 March 2012; pp. 219–234.
31. Zhou, S.Q.; Ni, R. Measurement of the specific heat capacity of water-based Al_2O_3 nanofluid. *Appl. Phys. Lett.* **2008**, *92*, 093123. [CrossRef]

32. Vajjha, R.S.; Das, D.K. Specific Heat Measurement of Three Nanofluids and Development of New Correlations. *J. Heat Transf.* **2009**, *131*, 071601. [CrossRef]
33. Li, L.; Zhang, Y.W.; Ma, H.B.; Yang, M. Molecular dynamics simulation of effect of liquid layering around the nanoparticle on the enhanced thermal conductivity of nanofluids. *J. Nanopart. Res.* **2010**, *12*, 811–821. [CrossRef]
34. Oh, S.H.; Kauffmann, Y.; Scheu, C.; Kaplan, W.D.; Ruhle, M. Ordered liquid aluminum at the interface with sapphire. *Science* **2005**, *310*, 661–663. [CrossRef]
35. Prasher, R.; Bhattacharya, P.; Phelan, P.E. Brownian-motion-based convective-conductive model for the effective thermal conductivity of nanofluids. *J. Heat Transf.* **2006**, *128*, 588–595. [CrossRef]
36. Xue, L.; Keblinski, P.; Phillpot, S.R.; Choi, S.U.S.; Eastman, J.A. Effect of liquid layering at the liquid-solid interface on thermal transport. *Int. J. Heat Mass Trans.* **2004**, *47*, 4277–4284. [CrossRef]
37. Starace, A.K.; Gomez, J.C.; Wang, J.; Pradhan, S.; Glatzmaier, G.C. Nanofluid heat capacities. *J. Appl. Phys.* **2011**, *110*, 124323. [CrossRef]
38. De Castro, C.A.N.; Murshed, S.M.S.; Lourenco, M.J.V.; Santos, F.J.V.; Lopes, M.L.M.; Franca, J.M.P. Enhanced thermal conductivity and specific heat capacity of carbon nanotubes ionanofluids. *Int. J. Therm. Sci.* **2012**, *62*, 34–39. [CrossRef]
39. Zare, V.; Moalemian, A. Parabolic trough solar collectors integrated with a Kalina cycle for high temperature applications: Energyy, exergy and economic analyses. *Energy Convers. Manag.* **2017**, *151*, 681–692. [CrossRef]